Composites Part A: Applied Science and Manufacturing 77 (2015) p. 106-113
DOI: 10.1016/j.compositesa.2015.06.018

Synchrotron radiation computed tomography for experimental validation of a tensile strength model for unidirectional fibre-reinforced composites

Y. Swolfs[1], H. Morton[2], A.E. Scott[2], L. Gorbatikh[1], P.A.S. Reed[2], I. Sinclair[2], S. M. Spearing[2], I. Verpoest[1]

[1] Department of Materials Engineering, KU Leuven, Kasteelpark Arenberg 44, 3001 Leuven, Belgium
[2] Material's Research Group, University of Southampton, University Road, Southampton, SO17 1BJ, United Kingdom

**Corresponding author: Y. Swolfs (yentl.swolfs@mtm.kuleuven.be), Tel. +3216373616.*

Abstract

Synchrotron radiation computed tomography has been used to analyse fibre break accumulation in unidirectional composites loaded in tension. The data are compared to model predictions. The model only slightly overestimated the composite failure strain, but predictions of fibre break density were too high, which can be mainly attributed to errors in the Weibull distribution. Both the number and percentage of interacting fibre break clusters were under-predicted by the model. This was attributed to an underestimation of stress concentrations in the model. While the experimental observations revealed mainly co-planar clusters, the model predicted mainly diffuse clusters. The experiments showed that the clusters did grow any further after their formation, while the model predicted a gradual development. Both local and dynamic stress concentrations were hypothesised to be key features for further exploration. The discrepancies identified, inform suggestions for directions advancing the state-of-the-art strength models of UD composites.

Keywords: **A:** Polymer-matrix composites (PMCs); **B:** Stress concentrations; **C**: Statistical properties/methods; **D**: Radiography;

1 Introduction

For any material to be used on a large scale in structural applications, the material behaviour needs to be understood in detail. Thus the understanding of damage initiation and propagation in composites, and the transition from subcritical to critical damage is vital [1, 2]. A common objective is to predict accurately the response of structures based on reliable material models. This will reduce the number of tests needed for design and validation. However, due to the lack of faith in the state-of-the-art models, they are implemented in an overly cautious way, leading to larger, heavier and more expensive composite structures than would otherwise be needed [3].

Experimental programs are thus needed to supplement the modelling results, and provide insight into the underlying mechanisms responsible for the observed failure

development [4]. This creates a strong driving force to combine physical modelling with experimental campaigns to enhance component design and material development [5].

The failure process of unidirectional (UD) composites in tension involves a sequence of events. Initially weak fibres break at relatively low loads, transferring their load to the surrounding fibres [6]. Failure is generally assumed to develop via the accumulation of individual fibre breaks due to the distribution in fibre strength, which then interact and grow into clusters of broken fibres [7]. Eventually a cluster of broken fibres reaches a critical size, triggering unstable crack propagation and final failure. Formation of the critical cluster is thus believed to be the strength-defining failure event [8-10].

Many theories exist to predict the tensile strength of UD composites [11-23], and most of these contain three key features. The first is the assumption of a Weibull distribution of fibre strength, which is determined by the random distribution of flaws in the fibre [23]. This feature is responsible for the progressive nature of damage in UD composites. The second feature is that stress is distributed from a broken fibre through the matrix, into the neighbouring, intact fibres. The third feature is the assumption that stress concentrations arise in these neighbouring intact fibres, which enhance the probability of neighbouring fibres failing once an individual fibre fractures [6]. The complexities of the stress transfer and redistribution mechanisms, combined with the statistical aspects of fibre strength, make modelling composite tensile strength a challenge [24].

Comprehensive experimental data are currently lacking, but are required to validate current models [25]. Previous experimental work has focused on single fibres [26-30] or model composites, analysed using scanning or Raman microscopy [30-32]. Their restriction to surface observations does not permit measurement of the bulk composite without sectioning, which has the inherent risk of introducing additional damage.

In the current work, synchrotron radiation computed tomography (SRCT) is used to analyse a carbon/epoxy $[90/0]_s$ laminate loaded *in situ* to failure. SRCT provides a three-dimensional representation of the material's internal structure at a resolution sufficient to identify individual broken fibres. *In situ* loading allows damage progression to be analysed. The work presented here compares the experimental data with the fibre-bundle model of Swolfs et al. [33-36]. A similar comparison has already been attempted in Scott et al. [37]. Their model predictions were reasonable at low applied strains, but seemed to diverge at higher strains. Their model was also less accurate at predicting clustering parameters, especially for larger clusters. This may have been caused by the inherent assumptions in their model. Firstly, Weibull data for a T600S carbon fibre were applied to model a T700S carbon fibre composite. The T600S data sheet quotes a failure strain of 1.8% [38], which is significantly lower than the 2.1% quoted for T700S [39]. Secondly, the model is only capable of predicting cluster sizes with a number of fibres equal to a power of 2. This hampers an accurate comparison between model and experiments, especially near final failure.

The present paper focuses on the accumulation of fibre breaks, and in particular the formation of clusters of broken fibres, as the development of a critical size of interacting fibre breaks is often assumed to be the strength-defining failure event for tensile loaded composites [8, 40]. The same experiments as in Scott et al. [37] were used, but the cluster pattern and growth were also tracked this time, leading to new insights in the

failure process. Conclusions are drawn by comparing the experimental and simulated results, leading to recommendations for further model development.

2 Materials and methods

2.1 Materials

$[90/0]_s$ Hexcel HexPly T700/M21 aerospace-grade carbon fibre/epoxy prepreg were provided by Airbus UK. They were used to manufacture composites with a fibre volume fraction of 55%. The 4mm wide double-notched coupons were prepared for tensile testing as described in Wright et al. [41]. Coupons were cut by abrasive water-jet, which previous research has shown induces no significant damage in similar specimens [41]. Notched samples were used as they enable the damage mechanisms close to final failure to be observed, because it constrains failure in a limited volume accessible by SRCT. The 90° plies delaminate from the 0° plies at 70% of the failure load and do not influence the failure development in the 0° plies. The section width between the notch roots was 0.8 mm, with an overall composite thickness of 1mm. This leads to a total of about 5500 0° fibres in the cross-section. Aluminium tabs were bonded to the specimen ends to aid loading, and to reduce stress concentrations at the loading ends. Ten specimens were tensile tested to failure in the 0° direction in a screw-driven load rig to determine the nominal failure load. A description of the rig and the testing methodology is provided in further detail in Wright et al. [41].

2.2 Synchrotron radiation computed tomography

Tomographic x-ray scans were undertaken on the ID19 beamline at the European Synchrotron Radiation Facility (ESRF), Grenoble France. A voxel resolution of 1.4 μm was used, which allowed the identification of individual fibres. A propagation distance of 37 mm allowed a degree of near-field Fresnel edge enhancement, which made it easier to identify individual fibre breaks. A tensile specimen was taken to seven different percentages of nominal failure load (40, 63, 70, 79, 84, 89, 94%) and scanned at each load step. The region incorporating the notch, with a total length of 2.3 mm was monitored. All breaks occurred within a length of 1.54 mm, which corresponds to a volume of 0.61 mm^3 for the 0° fibre plies. This length and volume were used in the strength model and in the normalisation of the break densities.

Data reconstruction was undertaken using in-house software at the ESRF. The break analysis was performed using VG-Studio™ and FIJI™. An example of the analysed volume is shown in Figure 1a, in which delaminations, matrix cracks due to 0° splitting and fibre breaks can all clearly be seen. Figure 1b and c show a fibre break in two orthogonal views, where the break is a distinct black zone. Breaks were quantified through visual inspection of the data files in at least two orthogonal planes to ensure accuracy, and extracted from the bulk composite.

Composites Part A: Applied Science and Manufacturing 77 (2015) p. 106-113
DOI: 10.1016/j.compositesa.2015.06.018

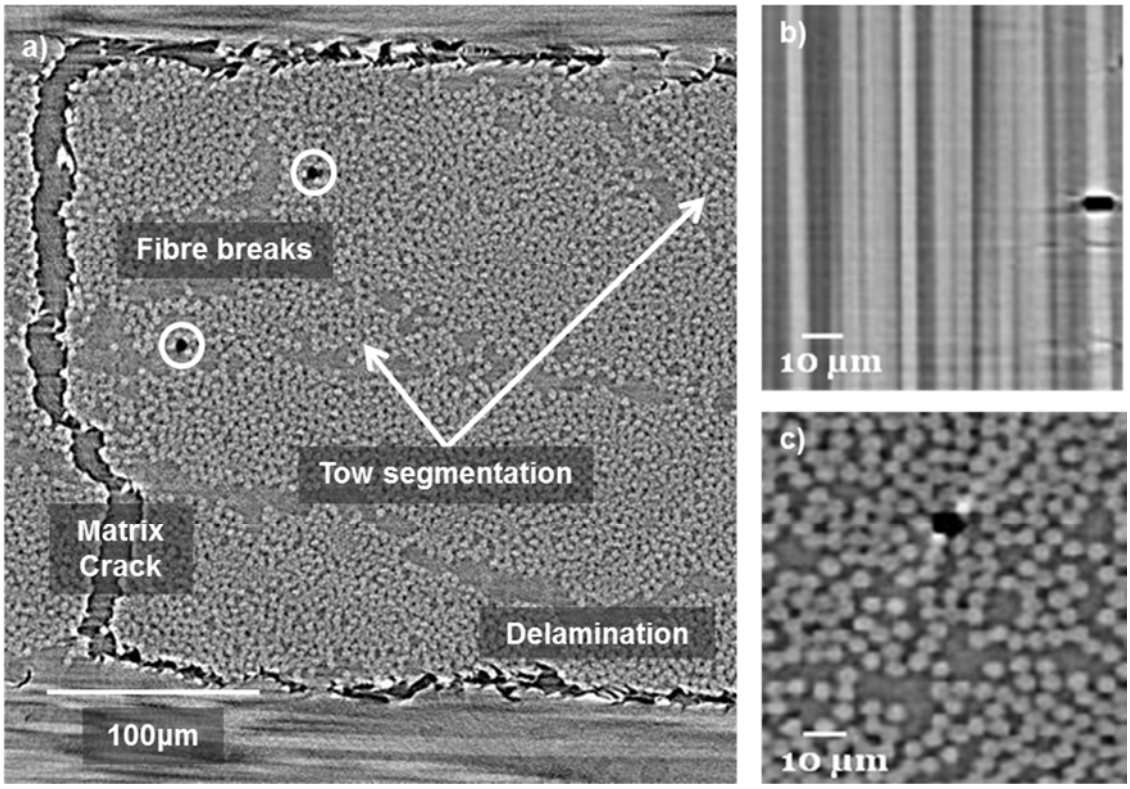

Figure 1: a) Cross-section of T700/M21 at the final load step (94% of final failure), showing fibre breaks in the 0° ply, delamination, matrix crack due to 0° splitting and tow segmentation. b) shows a fibre break with the loading direction being vertical, and (c) shows the same fibre break in a cross-section.

3 Model description

3.1 General description

The model is based on Rosen's chain-of-bundles approach [14] and has already been extensively described [33-36]. Each fibre was divided into fibre elements, which were assigned a Weibull strength according to their length. A bimodal Weibull distribution, which is based on the assumption of two competing flaw distributions, was chosen. This distribution is described by [42]:

$$F\left(\sigma_f\right) = 1 - \exp\left[-\frac{L}{L_0} \cdot \left(\frac{\sigma_f}{\sigma_{01}} \right)^{m_1} - \frac{L}{L_0} \cdot \left(\frac{\sigma_f}{\sigma_{02}} \right)^{m_2} \right] \quad (1)$$

in which σ_f is the fibre strength, L the element length, L_0 the reference gauge length, σ_{01} and σ_{02} the Weibull scale parameters for the first and second flaw distributions respectively, and m_1 and m_2 the Weibull moduli or shape parameters for the first and second flaw distributions respectively. The Weibull parameters are: $L_0 = 10mm$ $\sigma_{01} = 5200MPa$, $m_1 = 4.8$ $\sigma_{02} = 6100MPa$, and $m_2 = 12.0$ [42]. This data set closely follows the recommendations of Swolfs et al.[36] for setting up an accurate and reliable Weibull distribution: testing a large number of fibres at very short gauge lengths. We therefore

consider this data set to be the most reliable one for T700S carbon fibres. It was based on 234 fragmentation tests.

Random fibre packings were created with the generator described in [43-45], which was extensively validated by Romanov et al. [46]. These random packings with a 0.8 x 1 mm cross-section contained 5500 fibres with 55% fibre volume fraction and a length of 1.54 mm. This rectangular cuboid model corresponds to the experimental parameters. Each fibre was divided into 440 fibre elements, meaning the element length L was equal to the fibre radius 3.5 μm. A total of 50 Monte Carlo simulations were performed.

A flowchart of the model procedure is provided in Figure 2. The methodology is based on the works of Curtin, Okabe and co-workers [11, 18, 47-49]. After assigning a Weibull strength to each fibre element, the global strain was incremented by 0.04%. The size of the strain increment is gradually reduced, until near final failure it becomes 0.0025%. The gradual refinement is used so as to optimise computational speed, combined with the aim of achieving an accurate prediction near final failure. After each strain increment, the stress in each fibre element was calculated by multiplying the applied strain, its stress concentration factor (SCF) and the secant modulus of the carbon fibre at the applied strain. The secant modulus was used to account for the non-linear tensile behaviour of carbon fibre. A 20% stiffness increase is assumed for every 1% strain, as suggested by Toyama and Takatsubo [50]. The local stiffness at 0.6% corresponded to the 230 GPa from the datasheet [39], as this value is measured between 0.5 and 0.7%. The same stiffness increase was used to calculate the experimental stress-strain diagram, where only the applied load could be measured.

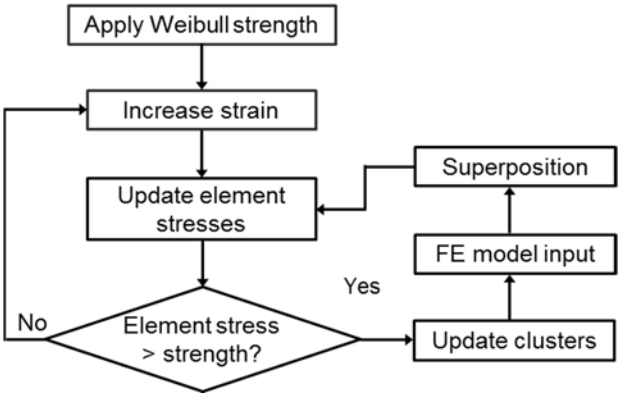

Figure 2: Flow chart for the strength model

If the element stress exceeded the element strength, then the element was considered broken. The cluster size was then updated for all fibre breaks, followed by an update of the SCFs and superposition of the SCFs in the nearby fibre elements. These SCFs and their superposition will be described in detail in the next two sub-sections. As the SCFs from a broken element may have caused additional elements to break, the model updates the element stresses and checks again whether any new elements have broken.

The process was repeated until no new fibre breaks were found at the particular strain level, the strain was then incremented and the process repeated. The model was stopped if an unstable propagation of fibre breaks was detected, found as a rapidly increasing

number of fibre breaks within the same strain increment. The clusters in the last strain increment were not calculated as this last strain increment was interrupted prior to the complete solution. The last strain before final failure is, however, only 0.0025% lower.

3.2 Finite element stress redistribution

This section gives a brief overview of the procedure used to calculate stress redistribution after a single fibre break, as previously described in detail in Swolfs et al. [43]. The FE model was used to calculate the full stress redistribution around a single broken T700S carbon fibre in a UD composite with a random fibre packing. While the strength model is a rectangular cuboid, the FE model is cylinder-shaped. The shape of the FE model does not affect the results, as the influence of the stress concentrations fades away quickly with distance from the centre.

The location of the individual broken fibre is referred to as the fibre break plane. The stresses in the broken fibre as well as in the surrounding intact fibres were extracted as a function of the distance along the fibre from this fibre break plane. The SCF was defined as the relative increase or decrease in average stress over the cross-section of a fibre due to the presence of the fibre break.

For the broken fibres, the average Gauss stress in the first layer of elements is used in combination with the points where 60%, 75%, 90% and 95% of the stress in the broken fibre is recovered. These points are chosen in such a way that piecewise linear interpolation leads to an accurate fit of the stress profile along the broken fibre.

Similarly, four points of interest are extracted for the intact fibres, as shown in Figure 3. In this case, the SCF value at each point of interest depends on the distance from the broken fibre. Therefore, these points were plotted as a function of that distance and linear, quadratic or logarithmic trend lines were fitted. This procedure is illustrated for the maximum SCF in Figure 4b. The equations of these trend lines were fed into the strength model and piecewise linear interpolation was used to reconstruct the stress profiles in the strength model.

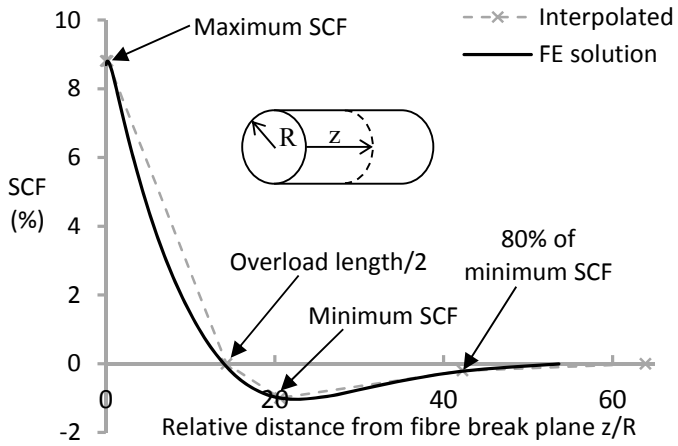

Figure 3: Illustration of the points of interest in the stress profile of the intact fibres. Piecewise linear interpolation is used in between these points.

For the M21 epoxy matrix, a tensile modulus of 1.26 GPa was provided by the manufacturer, with an assumed Poisson's ratio of 0.4. All materials were assumed to be linear elastic and perfectly bonded. The approach in [43] was further extended by incorporating a matrix crack in the plane of the fibre break. This matrix crack was also observed in the experimental data, but precise information on its size and shape could not be obtained. The FE model indicated that the exact size of the matrix crack did not have a significant influence on the predicted stress redistribution [34]. Therefore, it was assumed that the matrix crack stopped in between the nearest fibres, as shown in Figure 4a. The resulting SCFs are shown in Fig. 4b.

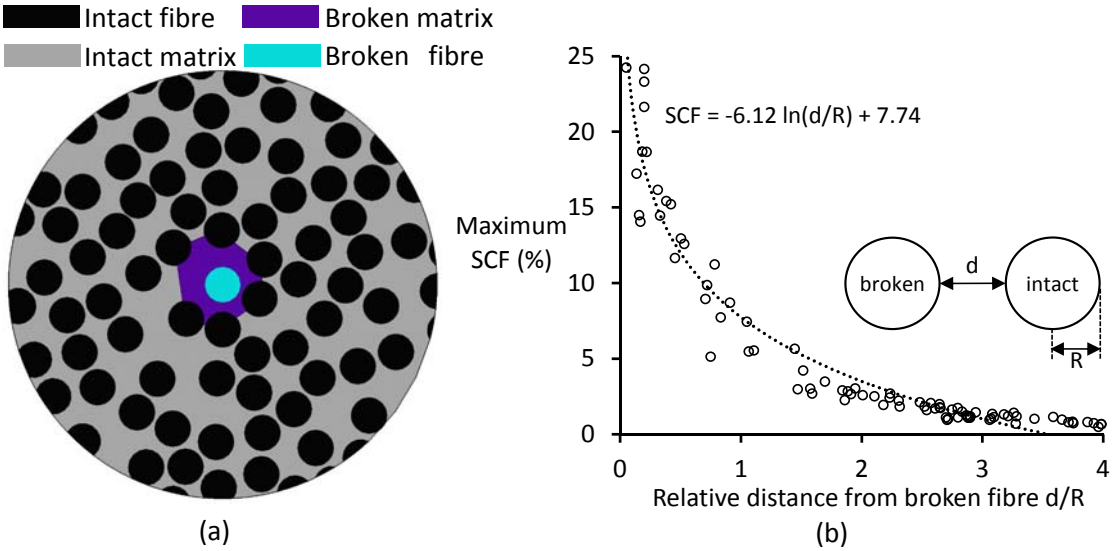

Figure 4: Matrix cracks around a single broken fibre: (a) Illustration of the matrix crack in the FE model, and (b) The stress concentration factors on intact fibres near a single, broken carbon fibre, as a function of the relative distance from the broken fibre.

Each fibre break is assumed to occur in the middle of an element in the strength model. This does not imply that the stress in that element will drop to zero, as stress recovery can already occur within the length of the element. Therefore, the element stresses were averaged over the length of each element. In this way, the stress profiles were entered accurately into the strength model prior to running it, without requiring FE calculations during the strength model. Since these profiles were averaged over five FE models, the SCFs that are applied in the strength model do not take into account the particular local geometry. This local geometry only has a small influence, as can be seen from the low scatter in the data in Figure 4b. Moreover, to keep the model computationally tractable, the SCFs were only applied to fibres with a surface-to-surface distance from the broken fibre of less than four fibre radiuses. Even though the SCFs on the other fibres were all lower than 1%, their omission still caused a total SCF of 10 to 15% to be neglected. To counteract these effects and ensure force equilibrium, the "missing" SCF was redistributed proportionally over the fibres within four fibre radiuses.

3.3 Superposition for multiple fibre breaks

The trend lines, such as the one in Figure 4b, incorporated the stress redistribution around a single broken fibre. When the strain is increased, however, new breaks appear

and clusters develop. When breaks are far apart they do not interact but when they are close, as in a cluster, the interactions become stronger. It is, however, impossible to use FE analysis to predict all possible cluster geometries. Therefore, the finite element model was developed for a single broken fibre, and superposition was used to account for these interactions. This approach predicts the SCFs around multiple fibre breaks based on the SCFs around single fibre break.

In the current model, an enhanced linear superposition was applied. Standard linear superposition would sum up the SCFs for single fibre breaks, even though it is known that the interactions between broken fibres in a cluster will cause an underestimation of the SCFs [19, 51]. Another issue is that this approach neglects the SCFs exerted by the broken fibres onto each other, resulting in a loss of force equilibrium in the model. The enhanced linear superposition rule proposed here starts off by applying standard linear superposition. The SCFs that are neglected in standard linear superposition and are caused by the SCFs that the broken fibres exert onto each other are redistributed over the nearby fibres. This redistribution was made in proportion to the SCFs predicted by standard linear superposition. This means that those fibres which carried a larger SCF in linear superposition also experience a larger fraction of the redistributed SCFs. This approach has been validated in Swolfs et al. [34].

4 Results and discussion

4.1 Macro-scale tensile response

Experimentally, it was difficult to achieve scans just before final failure, as the sample strength is unknown a priori. The highest strain, for which a SRCT image was obtained, was 1.80%, close to the ultimate failure strain of this particular sample of 1.89%. The stress-strain response predicted by the model and measured in the experiments is compared in Figure 5. The specimen response was linear until failure, consistent with the dominant role of the linear elastic fibres, and the relatively low number of broken fibres occurring before failure. The ultimate failure strain predicted by the model was $2.17 \pm 0.02\%$ which was higher than the experimentally measured failure strain of 1.89%. The reason for this difference is presumed to be due to an underestimation by the model of the cluster development at strains approaching failure. This will be explored in detail in the next sections.

Composites Part A: Applied Science and Manufacturing 77 (2015) p. 106-113
DOI: 10.1016/j.compositesa.2015.06.018

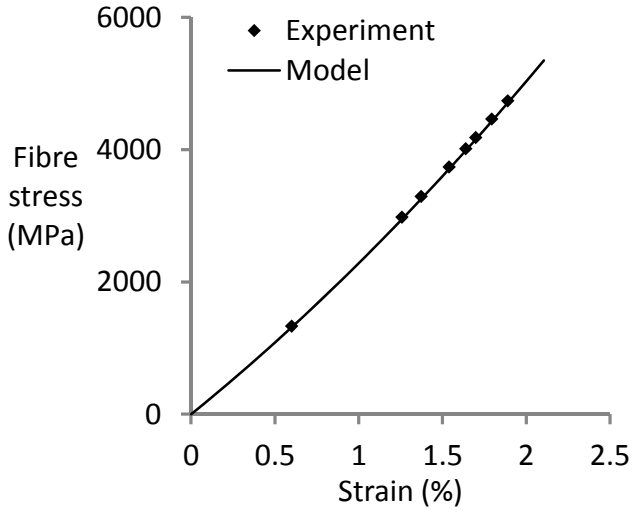

Figure 5: Stress-strain diagram of the model and the experiment data points.

4.2 Fibre break density

The fibre break density as a function of strain is shown in Figure 6. Experimentally, very few fibres within the composite break before final failure; in a specimen with 5500 fibres, there were fewer than 500 broken fibres/mm³ at the last loading increment prior to failure, meaning that less than 10% of the fibres were broken. Significant numbers of fibre breaks only accumulated at strains above approximately 1.6% at an increasing rate with applied strain (i.e. a power law relationship).

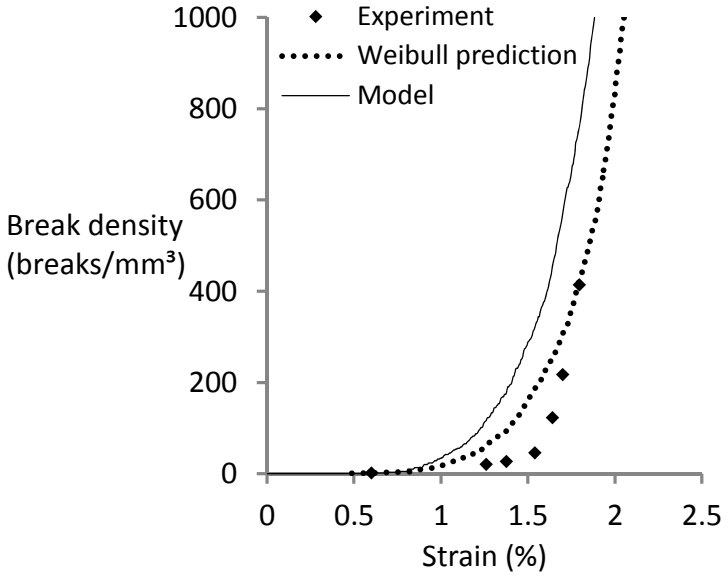

Figure 6: Accumulation of fibre break density as a function of applied strain. The prediction based on the Weibull data set is also added.

At these low fibre break densities, it is useful to compare the *in situ* fibre failure in the composite with that which would occur if the fibre failure was determined solely according to a Weibull distribution without any additional stress concentration or stress

transfer around breaks. This estimate of fibre break accumulation, together with that due to the model is shown in Figure 6. Both the model and the direct application of the Weibull data over-predict the break density, particularly at lower strains. In reality, broken fibres cause SCFs and increase failure probabilities, and hence the model exhibits a larger over-prediction. The fact that the Weibull data over-predicts the experimental data suggests that the Weibull distribution is inaccurate. Alternatively, the presence of the composite matrix might also reduce the *in situ* defect sensitivity of the fibres when they are surrounded by matrix. While the explanation of a reduced *in situ* defect sensitivity is speculative, inaccuracies in the Weibull distribution are commonly described in literature [23, 36, 42, 52-58].The literature has not yet settled on the most reliable measurement method for the distribution of fibre strength [42, 56-58]. Similarly, the most appropriate probability distribution function is still the subject of discussion. Modified versions of the Weibull distribution include the bimodal distribution [42, 57], the Weibull of Weibull distribution [23] and the power law accelerated Weibull model [23, 53].

The model prediction and the experimental break density measurements converge at strains above 1.8% (i.e. near failure). This may simply be a result of the in situ Weibull strength distribution being narrower than that measured from virgin and extracted fibres, due to some, as yet unexplained influence of the matrix. It is also consistent with observations made in the next section that cluster formation is under-predicted by the model, which is known to be an important factor in determining failure.

4.3 Cluster evolution

The occurrence of groups of interacting fibre breaks, termed a cluster, indicates the important role of local load sharing in the accumulation of damage. In the experimental work, a cluster was defined as two or more breaks in neighbouring fibres, separated axially by less than the ineffective length. This ineffective length was estimated previously in [59]. Correspondingly, in the model two broken fibre elements were considered as a cluster if (1) the surface-to-surface distance d between the fibres (see Figure 4b) was smaller than twice the fibre radius, and (2) the axial distance between break planes was less than ten times the fibre radius, which corresponds approximately to 90% stress recovery in the broken fibre. Whilst these definitions are not exactly the same, they are sufficiently similar to allow a useful comparison between the model predictions and experimental results. A sensitivity analysis for both the modelling and experimental procedure revealed that the exact definition had little effect on the cluster determination. Three different cluster parameters are analysed: cluster pattern, accumulation, and growth.

4.3.1 Cluster patterns

Experimental work identified two different cluster patterns: diffuse clusters (Figure 7a) and co-planar clusters (Figure 7b). The co-planar clusters were defined as clusters of breaks with an axial separation of less than a fibre radius (3.5μm), whilst diffuse clusters were those with an axial offset greater than this value. Approximately 70% of the clusters found experimentally were co-planar, while the model predicted only 20-30% co-planar clusters. This low percentage predicted by the model can be explained based on the stress profiles in the fibres near fibre breaks. While the stresses reach their

maximum in the fibre break plane, the stresses remain high over several fibre radii from the fibre break plane. This smeared out stress increase results in a finite failure probability of the fibre over this distance, and hence allowing diffuse clusters.

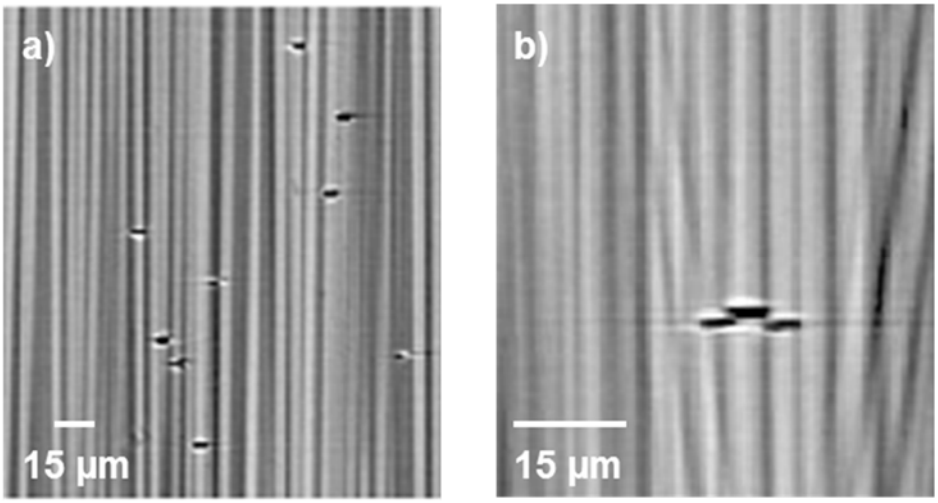

Figure 7: SRCT image of (a) diffuse, and (b) co-planar clusters.

The higher percentage of co-planar clusters in the experiment is difficult to explain based on previous work reported in the literature. Similar axial alignment of fibre breaks was also noticed by Van den Heuvel et al. [60], but an explanation for this feature was not offered. We propose two tentative hypotheses that could potentially explain a higher percentage of co-planar clusters. Both hypotheses are challenging to model and are currently not taken into account in any state-of-the-art model. Firstly, the dynamic SCFs, which occur when a fibre breaks and springs back [61], were not incorporated into the model. Secondly, very high stress gradients may occur across the fibres, originating at the tip of the matrix crack. For example, the FE model predicted local longitudinal stresses equivalent to a 260% SCF in a fibre close to the broken fibre, while the SCF averaged over the cross-section was only 23%. According to the Weibull distribution, very small volumes are expected to have a very high strength. It is questionable whether the Weibull distribution is still valid in such small volumes and with such high stress gradients, given that the characteristic length scales of the stress redistribution may approach the strength-controlling flaw size. The local microstructure of the fibres will also play a key role. Incorporating matrix plasticity into the FE model will tend to reduce these high local SCFs, but they will undoubtedly remain higher than the calculated average SCF value.

4.3.2 Cluster accumulation

In situ loading allows for the damage progression and the accumulation of clusters to be quantified. In calculating the number of breaks in clusters, each break in a cluster was counted instead of only counting the number of clusters. For example, a 3-plet contributed three breaks to the overall break count.

The largest cluster found experimentally was a 14-plet at a strain of 1.80%. At the same strain, the largest cluster size in the model was predicted to be between 2 and 4 (varying between individual Monte Carlo simulations). It may be more relevant to compare the

14-plet with the largest predicted cluster in the last strain increment before final failure. The average size of the largest predicted cluster in the last strain increment was 16. This size corresponds well with experimentally found 14-plet.

The accumulation of clusters as a function of strain is shown in Figure 8. As expected from Figure 6, the number of 1-plets is overestimated by the model. The number of clusters, however, is consistently underestimated and predicted to start only at higher strains. As noted in 4.3.1, this suggests that in the experiments the effective stress concentration is higher than allowed for in the model.

In the experiments, up to 50% of the total breaks occurred in clusters. However, there was no correlation between this cluster percentage and the applied strain. Higher strains did not always result in higher cluster percentages. In the model, the cluster percentage gradually increases with strain, but never reaches more than 30%. This difference may again be explained by the two effects suggested in "4.3.1 Cluster patterns".

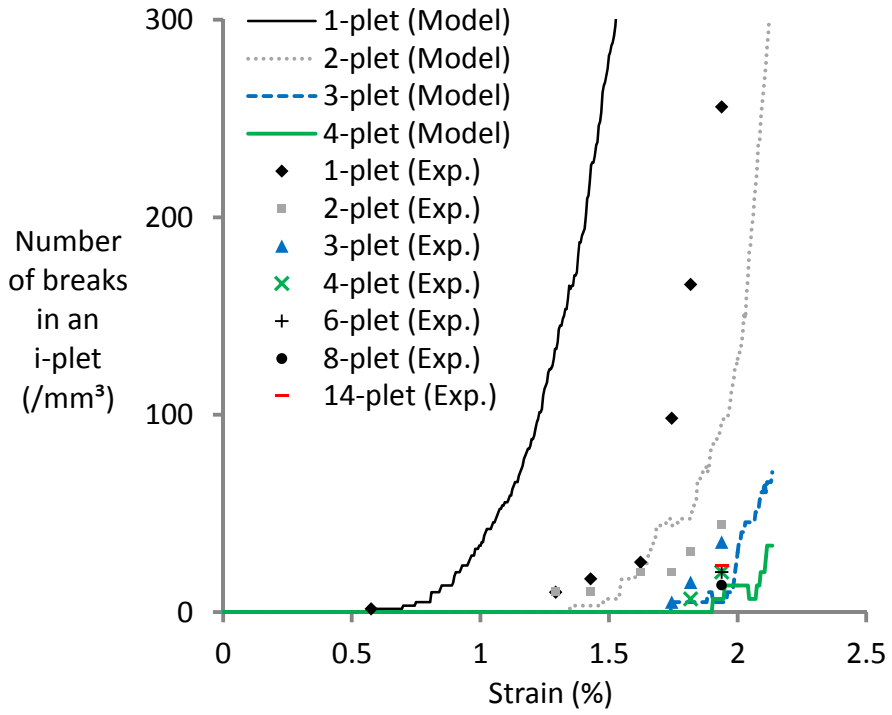

Figure 8: i-plet accumulation as a function of applied strain. Values were normalised to the experimental sample volume.

4.3.3 Cluster growth

The experimental results showed that as larger clusters formed there was no reduction in the number of smaller clusters. This may imply that clustering is a dynamic process and that once formed, clusters are unlikely to grow in size. To verify this hypothesis, all clusters in the experiment were tracked through the different strain increments. It was found that clusters formed at one particular strain increment and stayed at the same size as the strain increased. Since clusters formed in a single strain increment and higher applied strains were insufficient to cause cluster growth, this suggests that the dynamic stress concentrations present when a cluster formed must have been of significant

magnitude. The model only included static stress concentrations and predicts that clusters grow gradually with increasing strain increments. This again suggests that incorporation of the dynamic nature of stress concentrations is crucial for an accurate prediction of the cluster growth. Unfortunately, there has been little effort in this area [61, 62].

4.4 Fitted Weibull distribution

In the previous section, the bimodal Weibull distribution of Watanabe et al. [42] was used. Unfortunately, the literature suggests significant uncertainty exists regarding the reliability of fibre strength data [36, 52, 57, 58]. An alternative approach would be to fit the fibre break density to the data in Fig. 6 by changing the Weibull parameters. This was attempted by modifying the Weibull shape and scale parameters of a unimodal Weibull distribution. A good fit of the fibre break density was obtained for $\sigma_0 = 5200MPa$, $m = 10$ and $L_0 = 10mm$ (see Fig. 9). The failure strain was 2.08% $\pm$ 0.01%, which is reasonably close to the experimental value of 1.89%. While the value for σ_0 may be realistic, a Weibull modulus of 10 seems to be rather high compared to experimentally measured values [63]. The cluster development was also analysed, and found to be significantly delayed compared to the experiments (see Fig. 10). Similarly, we found the percentage of co-planar clusters remaining below 20%, which is significantly lower than our experimental observations.

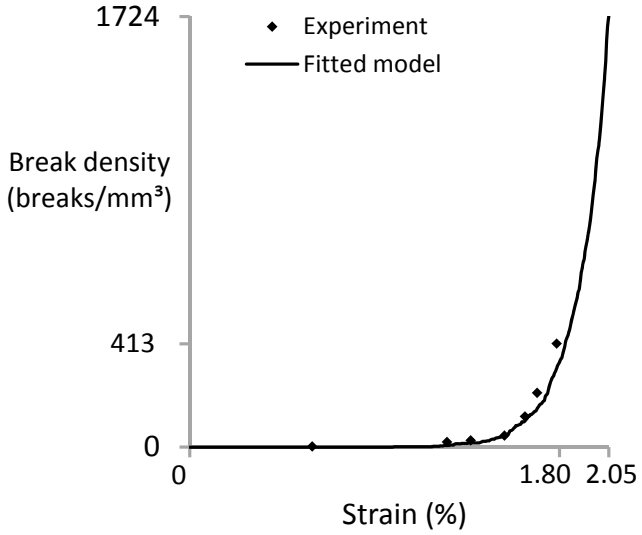

Figure 9: Excellent agreement in fibre break density for the experiments and the model with a fitted unimodal Weibull distribution.

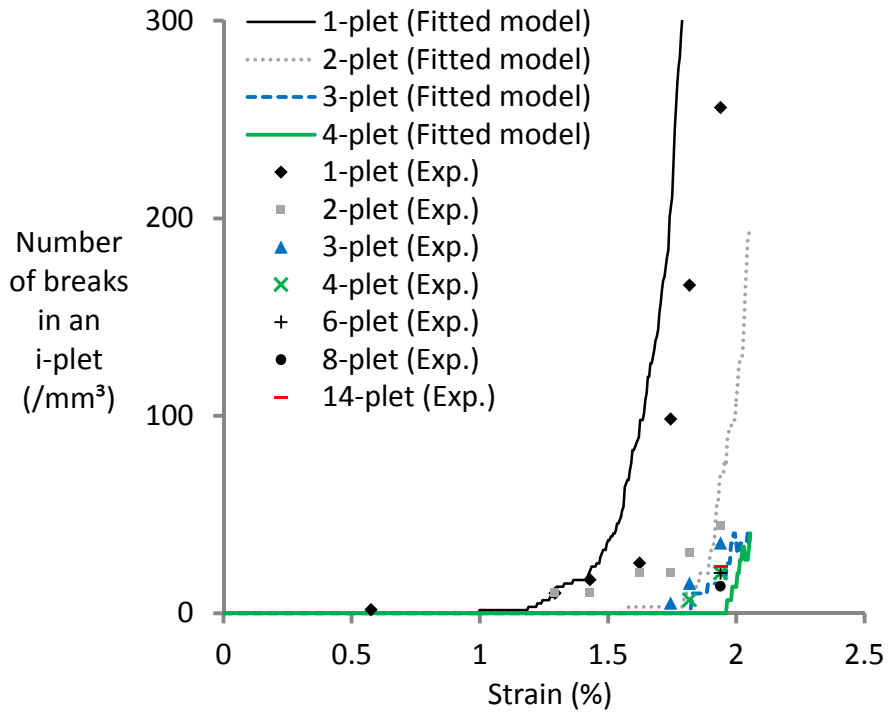

Figure 10: i-plet accumulation as a function of applied strain for the experiments and the fitted model. Values were normalised to the experimental sample volume.

This again emphasises our earlier conclusions that state-of-the-art strength models donot yet capture all the relevant physical mechanisms. Several hypotheses have been formulated that could potentially resolve these discrepancies.

5 Conclusions

The failure behaviour of unidirectional composites has been investigated by comparing synchrotron radiation computed tomography data to the results of a strength model. The model predicted the final failure strain and strength of the UD composite reasonably well, with only a small overestimation. The accumulation of break density with applied strain was overestimated by the model. This was attributed to errors in the Weibull strength distribution coupled with a potential reduction of the defect sensitivity of the fibres when they are surrounded by matrix.

The comparison based on the cluster pattern was a novel aspect in both the experiments and the model. The model predicted that diffuse clusters would dominate, whilst co-planar clusters were dominant in the experiments. The largest experimentally-observed cluster was a 14-plet, while the model predicted that ~16-plets would occur before final failure. The model predicted the development of large clusters to occur at higher strains, which is consistent with an underestimation of the stress concentrations. More measurements would be needed to confirm the probability of finding such a 14-plet, as only a single occurrence was found in the experiments.

Another crucial difference between the model and the experimental observations was the formation of clusters. In the experiments, clusters formed within a single load step and did not increase in size upon further loading. This is in contrast with the modelling

predictions, in which clusters gradually grew in size as strain was incremented. Two tentative hypotheses were formulated that could explain the observed discrepancy: the effect of dynamic stress concentrations and local stress concentrations at the matrix crack tip. These two effects are neglected by state-of-the-art strength models, but the presented results prove that they merit further attention. Even a Weibull distribution fitted to the experimental fibre break density could not resolve these discrepancies. More experiments are being planned to reveal this effect more clearly.

Future work will analyse how these effects influence the modelling predictions and whether they can narrow the discrepancies between modelling predictions and experimental data. Further experiments have also been performed on other fibre-matrix combinations to assess how this affects cluster development.

6 Acknowledgements

The work leading to this publication received funding from the European Union Seventh Framework Programme (FP7/2007-2013) under the topic NMP-2009-2.5-1, as part of the project HIVOCOMP (grant agreement n° 246389). The authors thank the Agency for Innovation by Science and Technology in Flanders (IWT) for grant funding for Y. Swolfs. The authors also thank A.R. Melro and P.P. Camanho for the permission to use their random fibre packing generator. I. Verpoest holds the Toray Chair in Composite Materials at KU Leuven. The authors gratefully acknowledge Luxfer Gas Cylinders Ltd., particularly Dr. Warren Hepples, and Airbus for materials supply. The authors acknowledge the staff at the ID19/ESRF beamline in Grenoble, and Dr. Mavrogordato at the μ-VIS X-ray Imaging Centre, Southampton.

7 References

[1] Bohse J. Acoustic emission characteristics of micro-failure processes in polymer blends and composites. Composites science and technology. 2000;60(8):1213-1226.
[2] De Greef N, Gorbatikh L, Godara A, Mezzo L, Lomov SV, Verpoest I. The effect of carbon nanotubes on the damage development in carbon fiber/epoxy composites. Carbon. 2011;49(14):4650-4664.
[3] Camanho PP, Maimi P, Davila CG. Prediction of size effects in notched laminates using continuum damage mechanics. Composites science and technology. 2007;67(13):2715-2727.
[4] Pineda EJ, Waas AM, Bednarcyk BA, Collier CS. Multiscale model for progressive damage and failure of laminated composites using an explicit finite element method. 11th Structures, structural dynamics, and materials conference, Palm Springs, California: AIAA; 2009.
[5] Beaumont PWR, Dimant RA, Shercliff HR. Failure processes in composite materials: getting physical. Journal of Materials Science. 2006;41(20):6526-6546.
[6] Nedele MR, Wisnom MR. Three-dimensional finite element analysis of the stress concentration at a single fibre break. Composites Science and Technology. 1994;51(4):517-524.
[7] Smith RL, Phoenix SL, Greenfield MR, Henstenburg RB, Pitt RE. Lower-tail approximations for the probability of failure of three-dimensional fibrous composites

with hexagonal geometry Proceedings of the Royal Society of London Series A: Mathematical Physical and Engineering Sciences. 1983;388(1795):353-391.
[8] Zweben C, Rosen BW. A statistical theory of material strength with application to composite materials. Journal of the Mechanics and Physics of Solids. 1970;18(3):189-206.
[9] Mahesh S, Phoenix SL, Beyerlein IJ. Strength distributions and size effects for 2D and 3D composites with Weibull fibers in an elastic matrix. International Journal of Fracture. 2002;115(1):41-85.
[10] Harlow DG, Phoenix SL. Probability distributions for the strength of composite materials II: A convergent sequence of tight bounds. International Journal of Fracture. 1981;17(6):601-630.
[11] Okabe T, Sekine H, Ishii K, Nishikawa M, Takeda N. Numerical method for failure simulation of unidirectional fiber-reinforced composites with spring element model. Composites Science and Technology. 2005;65(6):921-933.
[12] Blassiau S, Bunsell AR, Thionnet A. Damage accumulation processes and life prediction in unidirectional composites. Proceedings of the Royal Society of London Series A: Mathematical Physical and Engineering Sciences. 2007;463(2080):1135-1152.
[13] Zweben C. Tensile failure of fiber composites. AIAA Journal. 1968;6(12):2325-2331.
[14] Rosen BW. Tensile failure of fibrous composites. AIAA Journal. 1964;2(11):1985-1991.
[15] Pimenta S, Pinho ST. Hierarchical scaling law for the strength of composite fibre bundles. Journal of the Mechanics and Physics of Solids. 2013;61(6):1337-1356.
[16] Mishnaevsky Jr L, Brøndsted P. Micromechanisms of damage in unidirectional fiber reinforced composites: 3D computational analysis. Composites Science and Technology. 2009;69(7-8):1036-1044.
[17] Landis CM, Beyerlein IJ, McMeeking RM. Micromechanical simulation of the failure of fiber reinforced composites. Journal of the Mechanics and Physics of Solids. 2000;48(3):621-648.
[18] Curtin WA. Dimensionality and size effects on the strength of fiber-reinforced composites. Composites Science and Technology. 2000;60(4):543-551.
[19] Behzadi S, Curtis PT, Jones FR. Improving the prediction of tensile failure in unidirectional fibre composites by introducing matrix shear yielding. Composites Science and Technology. 2009;69(14):2421-2427.
[20] Mishnaevskyjr L, Brondsted P. Micromechanical modeling of damage and fracture of unidirectional fiber reinforced composites: A review. Computational Materials Science. 2009;44(4):1351-1359.
[21] Foreman JP, Behzadi S, Porter D, Jones FR. Multi-scale modelling of the effect of a viscoelastic matrix on the strength of a carbon fibre composite. Philosophical Magazine. 2010;90(31-32):4227-4244.
[22] Noda J, Nakada M, Miyano Y. Temperature dependence of accumulation of fiber breakages under tensile loading for unidirectional CFRP laminates. Journal of Reinforced Plastics and Composites. 2008;27(10):1005-1019.
[23] Curtin WA. Tensile strength of fiber-reinforced composites: III. Beyond the traditional Weibull model for fiber strengths. Journal of Composite Materials. 2000;34(15):1301-1332.

[24] Chohan, Galiotis C. Interfacial measurements and fracture characteristics of 2D microcomposites using remote laser Raman microscopy. Composites Part A: Applied Science and Manufacturing. 1996;27(9):881-888.
[25] Whiteside MB, Pinho ST, Robinson P. Stochastic failure modelling of unidirectional composite ply failure. Reliability Engineering & System Safety. 2012;108(0):1-9.
[26] Pegoretti A, DellaVolpe C, Detassis M, Migliaresi C, Wagner HD. Thermomechanical behaviour of interfacial region in carbon fibre/epoxy composites. Composites Part A-Applied Science and Manufacturing. 1996;27(11):1067-1074.
[27] Quek MY. The single fiber pull-out test analysis: influence of a compliant coating on the stresses at bonded interfaces. Journal of Adhesion Science and Technology. 1998;12(12):1391-1412.
[28] Andersons J, Joffe R, Hojo M, Ochiai S. Fibre fragment distribution in a single-fibre composite tension test. Composites Part B: Engineering. 2001;32(4):323-332.
[29] Ageorges C, Friedrich K, Ye L. Experiments to relate carbon-fibre surface treatments to composite mechanical properties. Composites Science and Technology. 1999;59(14):2101-2113.
[30] Marston C, Gabbitas B, Adams J, Marshall P, Galiotis C. Measurement of stress concentration around fibre breaks in carbon-fibre/epoxy-resin composite tows. Composites Science and Technology. 1997;57(8):913-923.
[31] van den Heuvel PWJ, vanderBruggen YJW, Peijs T. Failure phenomena in multi-fibre model composites .1. An experimental investigation into the influence of fibre spacing and fibre-matrix adhesion. Composites Part A: Applied Science and Manufacturing. 1996;27(9):855-859.
[32] Pickering KL, Bader MG, Kimber AC. Damage accumulation during the failure of uniaxial carbon fibre composites. Composites Part A: Applied Science and Manufacturing. 1998;29(4):435-441.
[33] Swolfs Y, McMeeking RM, Gorbatikh L, Verpoest I. The effect of fibre dispersion on initial failure strain and cluster development in unidirectional carbon/glass hybrid composites. Composites Part A: Applied Science and Manufacturing. 2015;69:279-287.
[34] Swolfs Y, McMeeking RM, Verpoest I, Gorbatikh L. Matrix cracks around fibre breaks and their effect on stress redistribution and failure development in unidirectional composites. Composites Science and Technology. 2015;108:16-22.
[35] Li L, Swolfs Y, Straumit I, Yan X, Lomov S. Cluster analysis of acoustic emission signals for 2D and 3D woven carbon fiber/epoxy composites. Submitted to Journal of Composite Materials. 2014.
[36] Swolfs Y, Verpoest I, Gorbatikh L. Issues in strength models for unidirectional fibre-reinforced composites: Weibull distributions, fibre packings and boundary effects. Composites Science and Technology, accepted. 2015.
[37] Scott AE, Sinclair I, Spearing SM, Thionnet A, Bunsell AR. Damage accumulation in a carbon/epoxy composite: Comparison between a multiscale model and computed tomography experimental results. Composites Part A: Applied Science and Manufacturing. 2012;43(9):1514-1522.
[38] T600S carbon fibre data sheet, www.toraycfa.com, 2014.
[39] T700S carbon fibre data sheet, www.toraycfa.com, April 2014.
[40] Ibnabdeljalil M, Curtin WA. Strength and reliability of fiber-reinforced composites: Localized load-sharing and associated size effects. International Journal of Solids and Structures. 1997;34(21):2649-2668.

[41] Wright P, Moffat A, Sinclair I, Spearing SM. High resolution tomographic imaging and modelling of notch tip damage in a laminated composite. Composites science and technology. 2010;70(10):1444-1452.
[42] Watanabe J, Tanaka F, Okabe T. The tensile strength distribution of carbon fibers at short gauge length. 38th Conference of the Japan Society for Composite Materials, 2013. p. 171-172.
[43] Swolfs Y, Gorbatikh L, Romanov V, Orlova S, Lomov SV, Verpoest I. Stress concentrations in an impregnated fibre bundle with random fibre packing. Composites Science and Technology. 2013;74:113-120.
[44] Swolfs Y, Gorbatikh L, Verpoest I. Stress concentrations in hybrid unidirectional fibre-reinforced composites with random fibre packings. Composites Science and Technology. 2013;85:10-16.
[45] Melro AR, Camanho PP, Pinho ST. Generation of random distribution of fibres in long-fibre reinforced composites. Composites Science and Technology. 2008;68(9):2092-2102.
[46] Romanov V, Lomov SV, Swolfs Y, Orlova S, Gorbatikh L, Verpoest I. Statistical analysis of real and simulated fibre arrangements in unidirectional composites. Composites Science and Technology. 2013;87:126-134.
[47] Okabe T, Nishikawa M, Takeda N, Sekine H. Effect of matrix hardening on the tensile strength of alumina fiber-reinforced aluminum matrix composites. Acta Materialia. 2006;54(9):2557-2566.
[48] Xia Z, Curtin WA, Okabe T. Green's function vs. shear-lag models of damage and failure in fiber composites. Composites Science and Technology. 2002;62(10-11):1279-1288.
[49] Okabe T, Takeda N, Kamoshida Y, Shimizu M, Curtin WA. A 3D shear-lag model considering micro-damage and statistical strength prediction of unidirectional fiber-reinforced composites. Composites Science and Technology. 2001;61(12):1773-1787.
[50] Toyama N, Takatsubo J. An investigation of non-linear elastic behavior of CFRP laminates and strain measurement using Lamb waves. Composites Science and Technology. 2004;64(16):2509-2516.
[51] Beyerlein IJ, Phoenix SL. Stress concentrations around multiple fiber breaks in an elastic matrix with local yielding or debonding using quadratic influence superposition. Journal of the Mechanics and Physics of Solids. 1996;44(12):1997-2039.
[52] Berger MH, Jeulin D. Statistical analysis of the failure stresses of ceramic fibres: Dependence of the Weibull parameters on the gauge length, diameter variation and fluctuation of defect density. Journal of Materials Science. 2003;38(13):2913-2923.
[53] Beyerlein IJ, Phoenix SL. Statistics for the strength and size effects of microcomposites with four carbon fibers in epoxy resin. Composites Science and Technology. 1996;56(1):75-92.
[54] Phoenix SL, Schwartz P, Robinson HH. Statistics for the strength and lifetime in creep-rupture of model carbon/epoxy composites. Composites Science and Technology. 1988;32(2):81-120.
[55] Otani H, Phoenix SL, Petrina P. Matrix effects on lifetime statistics for carbon fiber/epoxy microcomposites in creep-rupture. Journal of Materials Science. 1991;26(7):1955-1970.
[56] Gulino R, Phoenix SL. Weibull strength statistics for graphite fibres measured from the break progression in a model graphite/glass/epoxy composite. Journal of Materials Science. 1991;26(11):3107-3118.

[57] Watanabe J, Tanaka F, Okuda H, Okabe T. Tensile strength distribution of carbon fibers at short gauge lengths. Advanced Composite Materials. 2014:1-16.
[58] Phoenix SL, Sexsmith RG. Clamp effects in fiber testing. Journal of Composite Materials. 1972;6(JUL):322-337.
[59] Scott AE, Mavrogordato M, Wright P, Sinclair I, Spearing SM. In situ fibre fracture measurement in carbon-epoxy laminates using high resolution computed tomography. Composites Science and Technology. 2011;71:1471-1477.
[60] van den Heuvel PWJ, Peijs T, Young RJ. Failure phenomena in two-dimensional multi-fibre microcomposites .2. A Raman spectroscopic study of the influence of inter-fibre spacing on stress concentrations. Composites Science and Technology. 1997;57(8):899-911.
[61] Ji X, Liu XR, Chou TW. Dynamic stress concentration factors in unidirectional composites. Journal of Composite Materials. 1985;19(3):269-275.
[62] Swolfs Y, Gorbatikh L, Verpoest I. Fibre hybridisation in polymer composites: a review. Composites Part A: Applied Science and Manufacturing. 2014;67:181-200.
[63] Naito K, Tanaka Y, Yang J-M, Kagawa Y. Tensile properties of ultrahigh strength PAN-based, ultrahigh modulus pitch-based and high ductility pitch-based carbon fibers. Carbon. 2008;46(2):189-195.